

A matched-filter technique with an objective threshold

Shiro Hirano¹, Hironori Kawakata¹, and Issei Doi²

¹Department of Physical Science, College of Science and Engineering, Ritsumeikan University, 1-1-1,

Nojihigashi, Kusatsu, Shiga, 525-8577, Japan.

²Disaster Prevention Research Institute, Kyoto University, Gokasho, Uji, Kyoto 611-0011, Japan.

Key Points:

- We developed an objective thresholding method for seismic event detection.
- We show that cross-correlation coefficients among waveforms do not necessarily follow a normal distribution.
- Even in the case, we can detect outliers reasonably and objectively on the basis of Akaike's information criterion and extreme value theory.

Index Terms

7230 Seismicity and tectonics

Keywords

- Seismicity
- Seismic event detection
- Waveform cross-correlation
- Matched-filter analysis
- Information criterion
- Extreme value statistics

Corresponding author: Shiro Hirano, s-hrn@fc.ritsumei.ac.jp

21 **Abstract**

22 We propose an objective threshold determination method for detecting outliers from
 23 the empirical distribution of cross-correlation coefficients among seismic waveforms.
 24 This method is aimed at detecting seismic signals from continuous waveform records.
 25 In our framework, detectability is automatically determined from Akaike’s Informa-
 26 tion Criterion (AIC). We applied the method of seismic signal detection to contin-
 27 uous records collected over 2 years. The results show that the maximum value of
 28 network cross-correlation coefficients sampled from each constant interval can be ap-
 29 proximated by the theory of extreme value statistics, which provides a parametric
 30 probability density function of maxima. Using the function, outliers can be consid-
 31 ered with a reasonable criterion.

32 **1 Introduction**

33 A matched-filter (MF) analysis, which is a technique for quantifying the simi-
 34 larity between continuous and template waveforms using the cross-correlation coef-
 35 ficient (CC), is efficient in detecting weak seismic signals embedded in continuous
 36 waveform records [Gibbons & Ringdal, 2006]. Many types of seismic events have
 37 been detected automatically using MF analysis: non-volcanic tremors and low fre-
 38 quency earthquakes [e.g., Shelly et al., 2007; Ohta & Ide, 2008; Aso et al., 2011],
 39 seismic swarms [e.g., Shimojo et al., 2014; Ohmi, 2015], and foreshocks and after-
 40 shocks [e.g., Bouchon et al., 2011; Kato et al., 2012; Doi & Kawakata, 2012, 2013].
 41 In general MF analyses, waveforms are regarded as seismic signals when the CC be-
 42 tween a template and continuous waveform exceeds a threshold value. The threshold
 43 value has occasionally been defined as a constant [Doi & Kawakata, 2012, 2013] or
 44 not specified [Bouchon et al., 2011]. However, given the possibility of relatively high
 45 CC values randomly occurring for microtremors, the threshold should be determined
 46 depending on the empirical frequency distributions of CC. In other previous stud-
 47 ies, the threshold value was defined as a constant factor multiplied by the standard
 48 deviation (σ) [Ohta & Ide, 2008; Aso et al., 2011] or the median absolute deviation
 49 (MAD) [Shelly et al., 2007]. Under this strategy, we can estimate the possibility of
 50 a false positive if a probability density function (PDF) of the CC is known. Thus,
 51 characteristics of the PDF should be investigated both theoretically and experimen-
 52 tally. Because event detection is a type of outlier detection, careful attention should

53 be given to the tails of the frequency distribution of CC; do they follow the Gaus-
 54 sian, exponential, or power law? Only Aso et al. [2011] showed that the tail follows
 55 a normal distribution in their case. In this study, we first derive a normal distribu-
 56 tion that the CC between random microtremor and random template waveform may
 57 follow and investigate the effect of a band-pass filter, which provides reference for
 58 determining a realistic CC distribution. Next, we consider a distribution that the
 59 maximum value of CC in every constant interval follows for robust outlier detection
 60 using non-random continuous waveform records. The distribution of maxima in ev-
 61 ery constant interval is given by the extreme value theory [Gumbel, 1958]. Subse-
 62 quently, we demonstrate that the tails of CC values are well modeled by the extreme
 63 value distribution rather than the normal distribution through a case study of 2-
 64 years continuous records and multiple templates of foreshocks before an M5.4 crustal
 65 earthquake in Japan. Given the extreme value distribution, we employ a reason-
 66 able method for detecting outliers based on Akaike’s Information Criterion (AIC).
 67 Although we focus on a specific foreshock activity in our data analysis section, the
 68 method proposed in this study is efficient for other seismic phenomena and regions.

69 2 Theory and Method

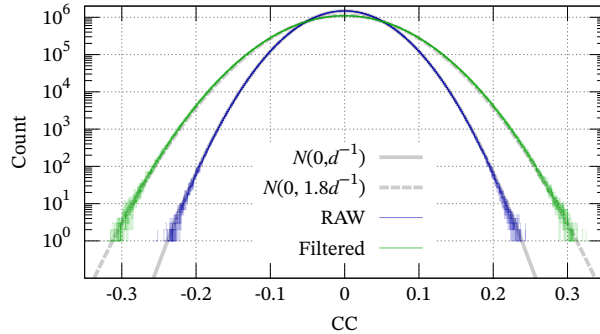
70 2.1 Ideal frequency distribution of CC

71 In the following, without loss of generality, we regard velocity seismograms as
 72 the data. The frequency distribution of CC between a continuous record and an ar-
 73bitrary template waveform array of length d follows a normal distribution whose
 74 mean is zero and variance is d^{-1} if the continuous record is an independent and
 75 identically distributed (i.i.d.) random variable. Let d -dimension vectors $\mathbf{u} := (u_i)$
 76 and $\mathbf{v} := (v_i)$ ($i = 1, 2, \dots, d$) be discretized and offset-eliminated waveform arrays of
 77 length d . Their CC is given as

$$78 \quad CC = \hat{\mathbf{u}} \cdot \hat{\mathbf{v}}, \quad (1)$$

79
 80 where $\hat{\mathbf{u}}$ and $\hat{\mathbf{v}}$ are normalized \mathbf{u} and \mathbf{v} , respectively, by their L_2 -norm. If \mathbf{v} is ex-
 81 tracted from a random waveform, the normalized vector $\hat{\mathbf{v}}$ is an isotropic random
 82 vector restricted on the $(d - 1)$ -dimensional unit sphere. Because eq.(1) is a projec-
 83 tion of $\hat{\mathbf{v}}$ along the $\hat{\mathbf{u}}$ -direction, CC can be regarded as a velocity component along
 84 the $\hat{\mathbf{u}}$ -direction of randomly hurtling particles with unit velocity ($|\hat{\mathbf{v}}| \equiv 1$). There-

85 fore, the PDF of CC can be approximated by extending the Maxwell-Boltzmann
 86 distribution from 3-dimensional space to d -dimensional space; see also Appendix
 87 A. In fact, the template and continuous waveform are filtered in MF analyses be-
 88 cause seismic waveforms have high S/N ratios in some limited frequency bands. Lin-
 89 ear band-passed filtering is equivalent to the convolution of a characteristic func-
 90 tion and the continuous waveform, and therefore, \mathbf{v} is not a complete random vector
 91 but necessarily has interdependence among some neighbor samples (referred to as
 92 “self-interdependence”) depending on the filter. Thus, we conducted numerical ex-
 93 periments; we calculate CC between an i.i.d. random waveform of length 10^8 and a
 94 random array of length $d = 500$ (figure 1). After 10 experiments, we confirmed that
 95 CC follows the normal distribution $\mathcal{N}(0, d^{-1})$ as expected above and in Appendix
 96 A. On the other hand, if we regard the waveforms as 100 Hz time-series and apply a
 97 band-pass filter of 5–30 Hz that is required in the next section, we find that the dis-
 98 tribution is approximated as $\mathcal{N}(0, 1.8d^{-1})$, as shown in figure 1. Therefore, we can
 99 conclude that CC follows the normal distribution even after applying the band-pass
 100 filter if the continuous waveform is random.



101 **Figure 1.** Frequency distribution of CC in a numerical experiment. CC between a raw ran-
 102 dom noise vs. a random template follows the normal distribution $\mathcal{N}(0, d^{-1})$, whereas CC be-
 103 tween a filtered random noise vs. the random template follows $\mathcal{N}(0, 1.8d^{-1})$.

104 2.2 Frequency distribution of the maximum of CC

105 The assumption of i.i.d. in the previous subsection might not be valid in cases
 106 where multiple similar earthquake events frequently occur, which radiates waveforms
 107 similar to the templates, or the microtremor repeats similar patterns. In such cases,

108 even accidentally, relatively high CC values appear around their local peaks because
 109 of the self-interdependence. Hence, the frequency distribution of all values of CC will
 110 be contaminated by the high values repeatedly, thus rendering the tail of the distri-
 111 bution wider and the interpretation more difficult. To avoid this problem, outliers
 112 should be detected from the maximum value of CC in every M sample by assum-
 113 ing that the self-interdependence of microtremors or seismic waveforms is lost within
 114 M samples. This assumption is valid because, in general, shorter-term correlation is
 115 stronger than longer-term correlation. Theoretically, it has been shown that the fre-
 116 quency of the maxima of any distribution in every interval follows the Generalized
 117 Extreme Value (GEV) distribution [Gumbel, 1958; Coles, 2001], which has been em-
 118 ployed to model possibilities of rare events, such as floods and economic crisis. GEV
 119 has the following cumulative density function (CDF):

$$120 \quad F_{\text{GEV}}(x | \mu', \sigma', k) = \exp \left(- \left(1 + k \frac{(x - \mu')}{\sigma'} \right)^{-1/k} \right), \quad (2)$$

121
 122 where x is a random variable, and μ', σ' and k are the location parameter, scale pa-
 123 rameter, and shape parameter, respectively. We have to note that $\text{sgn}(k)(x - \mu' + \sigma'/k) \geq$
 124 0 must be satisfied; otherwise the possibility is defined to be zero. It may be pos-
 125 sible to detect outliers by fitting the distribution of the maxima with GEV even if
 126 CC does not follow the normal distribution while their maxima follow GEV; see Ap-
 127 pendix C for the maximum likelihood estimation (MLE) of the GEV parameters. In
 128 particular, if every interval contains a sufficient amount of data, the cumulative dis-
 129 tribution converges to one of 3 specific cases depending on the shape of their tail:
 130 the Gumbel distribution, Fréchet distribution, or Weibull distribution. In the next
 131 section, we assume that they can be approximated by the CDF of the Gumbel distri-
 132 bution:

$$133 \quad F_{\text{G}}(x | \mu', \sigma') := \lim_{k \rightarrow 0} F_{\text{GEV}}(x | \mu', \sigma', k) \quad (3)$$

$$134 \quad = \exp \left(- \exp \left(- \frac{x - \mu'}{\sigma'} \right) \right).$$

135 This is because of the following reasons: 1) as confirmed in the next section, the ac-
 136 cumulated data distribution shows straight falloff in semi-log plots, which is a char-
 137 acteristic of the Gumbel distribution, and 2) as in Appendix C, MLE of three pa-
 138 rameters for GEV is technically difficult in some case. We focus on and plot $1 - F_{\text{G}}$
 139 in the following.

140

2.3 Method for event detection

141

142

143

144

145

146

147

148

149

150

151

152

153

154

155

156

157

158

159

160

161

162

163

164

165

166

167

168

169

170

171

172

Although the threshold for MF analyses has widely been assumed from the histogram of data, we have no unified or objective algorithm to assume an appropriate value of the threshold. Here, we propose an algorithm for detecting outliers reasonably and objectively on the basis of an information criterion. The elimination of outliers for minimizing AIC has been developed in applied statistics [Kitagawa, 1979; Ueda, 1996, 2009; Marmolejo-Ramos et al., 2015] and implemented in bioinformatics [Kadota et al., 2003]. Kitagawa [1979], Ueda [1996, 2009], and Kadota et al. [2003] assumed that the random variable other than the outliers follows a normal distribution and calculated AIC; Marmolejo-Ramos et al. [2015] investigated the applicability of the method in non-Gaussian and skewed distribution cases. We assume the Gumbel distribution and calculate the difference in AIC when we increase the number of suspects, which indicates whether the increment of the number is reasonable.

We sort N data in the descending order ($x_1 > x_2 > \dots > x_N$) and assume that the leading s data (x_1, x_2, \dots, x_s) are outliers that do not follow the Gumbel distribution while other $N - s$ data are sampled from the same Gumbel distribution. Note that, unlike our notation, N data were sampled from the population distribution and number of all data was $N + s$ in Ueda [1996, 2009]. Then, AIC with the s outliers is represented as

$$\frac{1}{2}\text{AIC}_s = - \sum_{j=s+1}^N \log f(x_j | \theta') - \log(N - s)! + s \quad (4)$$

[Ueda, 1996, 2009; Marmolejo-Ramos et al., 2015], where f is the assumed PDF the samples follow, and θ' is the maximum likelihood parameters. In the original method, f has been assumed to be the normal distribution [Ueda, 1996, 2009]. However, the original method tends to be sensitive and detect too many values as outliers if the true distribution is positively skewed [Marmolejo-Ramos et al., 2015]. In our case, we assume that the true distribution is approximated by the Gumbel distribution that has positive skewness. Therefore, instead of the normal distribution, $f(x_j | \theta) = P_G(x_j | \mu', \sigma')$ should be considered, where $P_G := \frac{dF_G}{dx}$ is the PDF of the Gumbel distribution.

In the following, we do not directly calculate eq.(4) that contains uncalculatable huge number $\log(N - s)!$ for our case ($N \sim 10^6$). Instead, for sufficiently large N , the difference in AIC between the cases of s outliers and $s + 1$ outliers, $\frac{1}{2}d\text{AIC}_s$,

173 can be approximated as

$$\begin{aligned}
 & \frac{1}{2}d\text{AIC}_s := \frac{1}{2}(\text{AIC}_{s+1} - \text{AIC}_s) \\
 & \sim \log P_G(x_{s+1} | \mu', \sigma') + \log(N - s) + 1.
 \end{aligned}
 \tag{5}$$

174
175
176 Strictly, the maximum likelihood parameters based on all N data could differ from
177 those estimated using $N - s$ or $N - s - 1$ data. However, we assume that $N \gg s$
178 holds and the parameters do not change significantly after the elimination of s data;
179 see also Appendix B on its effect. Because we focus on the right tail of P_G and x_i is
180 in the descending order, $P_G(x_s) < P_G(x_{s+1})$ holds, which results in

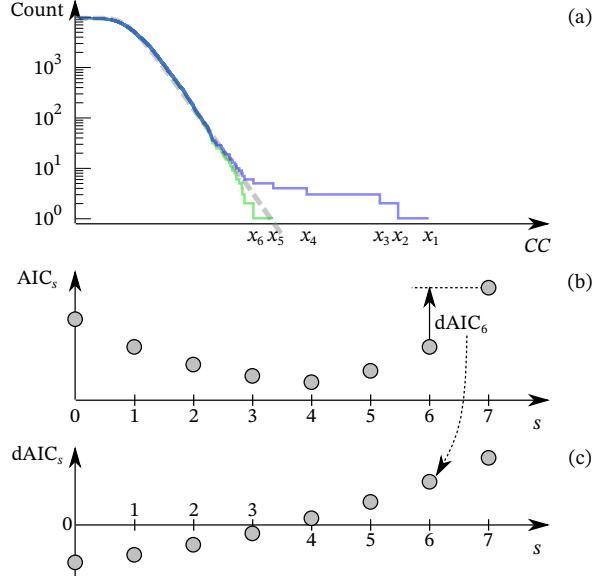
$$\frac{1}{2}d\text{AIC}_s < \frac{1}{2}d\text{AIC}_{s+1}.
 \tag{6}$$

181
182
183 In other words, the difference in AIC is a monotonically increasing sequence. If $d\text{AIC}_s <$
184 0 holds, from the definition, we can reasonably regard that x_{s+1} is also an outlier
185 rather than a sample from the Gumbel distribution. On the contrary, if $d\text{AIC}_s > 0$
186 holds, the monotonicity guarantees that the difference is always positive as s in-
187 creases. Thus, all x_i ($i > s$) are not outliers. Finally, our procedure schematically
188 illustrated in Figure 2 is as follows. We first obtain the MLE of the parameters μ'
189 and σ' , and then calculate $d\text{AIC}_s$ for $s = 0, 1, 2, \dots$. We stop the calculation when s
190 reaches s_0 , which makes $d\text{AIC}_s$ positive for the first time, and finally conclude that
191 x_1, x_2, \dots, x_{s_0} are outliers.

199 3 Case Study

200 3.1 Data

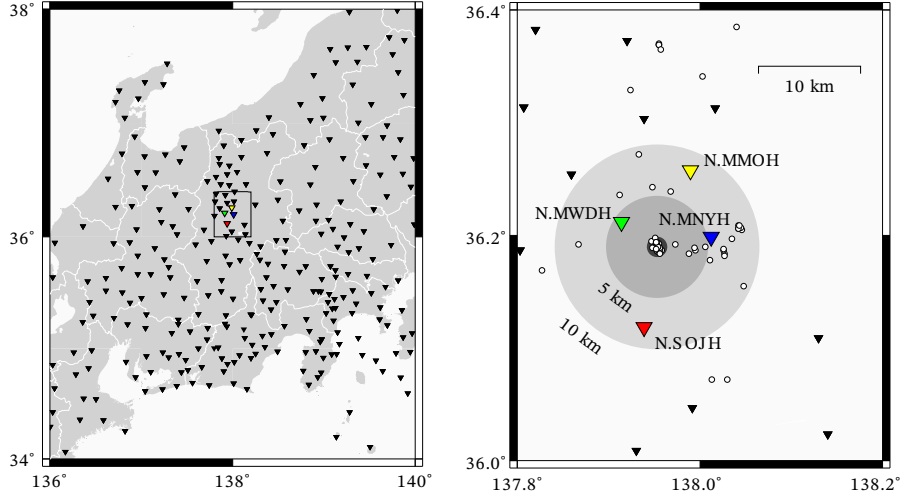
201 We considered a foreshock sequence of an M5.4 earthquake: origin time =
202 2011-06-30 08:16:37:06(JST); epicenter = 35.188N, 137.955E; depth = 4.3 km. Ac-
203 cording to the JMA catalog, 27 small foreshocks were recorded within 13 h before
204 the mainshock (Table S.1); their epicenters are within 1 km from the epicenter of
205 mainshock and surrounded by 4 Hi-net observation stations within 10 km (Figure
206 3), which may enable us to investigate the seismicity precisely. Thus, for each sta-
207 tion and component, the 27 template waveforms were extracted from 0.5 s before
208 each arrival of P-wave, and their length was 5 s (= 500 samples), such that the sig-
209 nificant part of S-wave and its coda are included. To search events similar to these
210 foreshocks, a criterion for outlier detection based on the empirical distribution of
211 CC is required. We thus calculated the Network Cross-correlation Coefficient (NCC)



192 **Figure 2.** Schematic illustration for estimating $s_0 = 4$, where s_0 is the number of outliers
 193 out of $N = 10^4$. (a) Cumulative number of raw data (blue steps), estimated Gumbel distri-
 194 bution (gray broken line), and cumulative number of data after elimination of x_1, \dots, x_{s_0}
 195 (green steps). (b) Dependence of AIC on the number of outlier candidates, s . (c) Dependence
 196 of $dAIC_s := AIC_{s+1} - AIC_s$ on s , where the definition is exemplified for $s = 6$. Even though
 197 the blue step due to x_5 is above the gray line in (a), x_5 is not regarded as the outlier because the
 198 step becomes closer to the gray line after the elimination.

212 among template waveforms due to the 27 events and 2-years continuous waveforms
 213 between 2009-06-29 and 2011-06-28 before the activation of the foreshocks. NCC
 214 is the averaged value of CC obtained in each station and component after shifting
 215 CC by lags between the origin time and arrival time of P-wave [Gibbons & Ringdal,
 216 2006]. Even after averaging, maxima of NCC should follow GEV because maxima
 217 generated by arbitrary distribution follow GEV [Gumbel, 1958; Coles, 2001]. In our
 218 case, we stack 12 CC time series based on 3 components of the 4 stations and ob-
 219 tain 27 histograms of NCC in total. Before the calculation, we applied a band-pass
 220 filter to focus on the frequency band, in which waveforms due to foreshocks show
 221 high S/N ratios. Although Doi & Kawakata [2012] applied a band-pass filter of 15–
 222 40 Hz, we applied the filter of 5–30 Hz depending on the spectra of template wave-
 223 forms; some automatic and objective determination method of the band should be
 224 developed in the future. We eliminated 15-s daily data of 09:00:00.00–09:00:15.00 for

225 checking the state-of-health of the observation instrument of Hi-net to ensure that
 226 CC was not affected by the test signals.

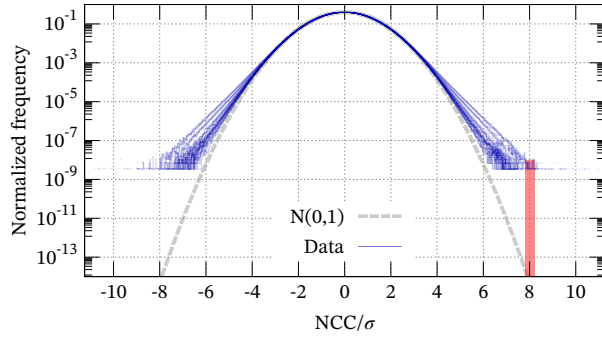


227 **Figure 3.** Distribution of observation points (triangles) and foreshock hypocenters (white circles)
 228 prior to an M5.4 mainshock in Nagano, Japan. Waveforms observed at N.MWDH (green),
 229 N.MNYH (blue), N.MMOH (yellow), and N.SOJH (red) stations were analyzed in this study. See
 230 Table S.1 for detail of the 27 events within 1 km from the epicenter shown in the darkest circle.

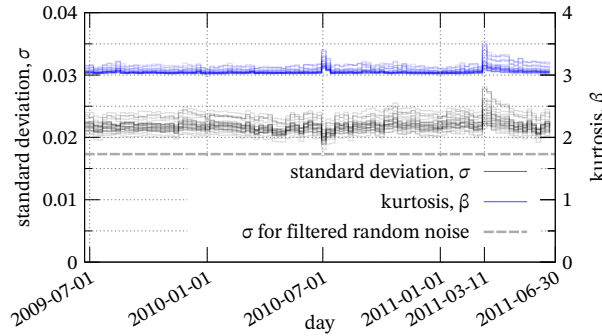
231 3.2 Result: Histogram of NCC

232 All histograms of NCC are shown in Figure 4. The histograms were normalized
 233 by their standard deviation, which means that they should be well approximated by
 234 the standard normal distribution plotted by the gray parabola in the semi-log plot
 235 if NCC follows a normal distribution. However, the tails of the NCC histograms ap-
 236 pear to be linear in the semi-log plot, and significantly different from the theoretical
 237 distribution discussed in the previous section. The difference between the theoretical
 238 model and empirical data is over a hundredfold in 7σ and ten thousandfold in 8σ .
 239 Therefore, the possibility of false positives may be severely underestimated if we set
 240 the threshold value as 8σ [Aso et al., 2011; Kato et al., 2012] and implicitly assume
 241 that the histogram follows a normal distribution. This fact strongly implies that the
 242 observed microtremor is significantly far from the i.i.d. assumed in the ideal case
 243 and has non-negligible self-interdependence. Weekly statistics of NCC histograms
 244 (Figure. 5) show that the standard deviation is higher than the case of the random

245 waveform ($\sigma = \sqrt{1.8d^{-1}}$, where $d = 500 \times 12$ in this case), which implies that
 246 the microtremor is somehow biased. Hence, we should refer to the distribution of
 247 the maxima of NCC that is less sensitive to the self-interdependence. Figure 5 also
 248 shows that characteristics of histograms, such as the standard deviation and kurtosis,
 249 fluctuated immediately after the week, including those on March 11, 2011, the
 250 day the M9.0 Tohoku earthquake occurred. However, the 2 years were not separated
 251 in our analysis because a sufficient amount of data is required to investigate the tails
 252 of histograms.



253 **Figure 4.** Empirical distribution of NCC between 2-years continuous records and 27 template
 254 waveforms (blue). The abscissa is normalized by the standard deviation. Vertical red bar indi-
 255 cates that the empirical distribution is several orders larger than the normal distribution (gray)
 256 in 8σ .



257 **Figure 5.** Temporal variation of the standard deviation and kurtosis of the empirical distribu-
 258 tion of NCC.

259

3.3 Result: Cumulative Distribution of max. of NCC

260

261

262

263

264

265

266

267

268

269

270

271

272

273

We attempted to detect seismic events that possibly occurred in the 2 years using the proposed method in 2.3 after fitting the cumulative number of the maxima of NCC at every minute between 2009-06-29 and 2011-06-28. In total, we could select 21 outliers according to Figure 6, which shows the cumulative number of calculated NCC, the estimated Gumbel distribution $1 - F_G(x | \mu', \sigma')$, and detected outliers. However, we classified some of these outliers as the same event because they emerged within 1 s. Finally, we could detect 4 new events, as shown in Table 1, which have not been cataloged by the JMA. As shown in Figure S.1–S.4, the detected waveforms show amplitudes of maximum 10–20% of the template waveforms and, therefore, have relatively low S/N ratios compared to the template. Even from such noisy data, our method provided the seismic signals without any prescribed threshold. The finding of the triplet similar events 3–4 days before the mainshock in the foreshock region (IDs B–D in Table 1) may provide us with new insight for considering the preparation process of the mainshock.

278

Table 1. Detected events by the proposed algorithm.

ID	date	time	similar to
A	2011-05-04	19:17:00	05, 06
B	2011-06-26	11:57:47	01, 02, 04, 14, 18, 27
C	2011-06-26	12:57:45	01, 02, 04, 18, 23, 27
D	2011-06-27	07:24:14	01, 02, 04, 18, 20, 23, 27

279

4 Discussion

280

281

282

283

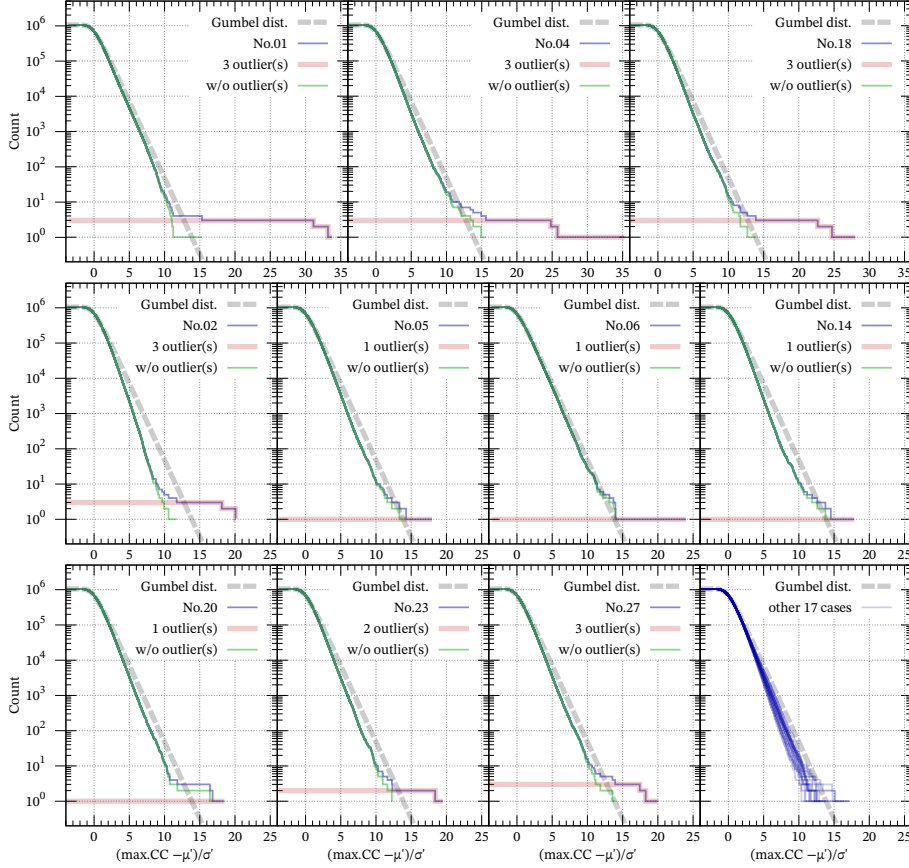
284

285

286

287

Compared to conventional thresholding methods, the most important advantage of our method is that the results are objective and reasonable; the result is less affected by arbitrariness in principle. We can suggest the possibility of false positives under the Gumbel distribution because the differences between the distribution and cumulative number of data are almost less than tenfold (Figure 6). The conventional method involves a trade-off between the number of detected events and false positive depending on the threshold value. In our method, however, the detection criterion is automatically determined depending only on the quality of data. Only 4 events were



274 **Figure 6.** Cumulative distributions of normalized NCC (blue) and the Gumbel distribution
 275 with $\mu' = 0$ and $\sigma' = 1$ as the fitting curve (gray) for 27 templates of Table S.1. Red steps indi-
 276 cate detected outliers in terms of the minimization of AIC. 17 cases accompanied by no outliers
 277 are plotted all together in the right bottom.

288 detected in our analysis, which may mean that the hypocenter region had been quite
 289 inactive before the foreshock activity or our method is excessively strict at finding
 290 many uncataloged events. Nevertheless, even if the latter is true, the detection of 4
 291 uncataloged events shows that our method has higher detection ability than that of
 292 JMA at that term, at least for similar seismic events.

293 It is noteworthy that our method is not completely free of arbitrariness. One
 294 concern is the length of intervals using which we selected the maxima. In our ex-
 295 periment, we selected an interval of 1 min (i.e., 6,000 samples) considering com-
 296 putational time, but in principle, the interval can be, for example, 5 seconds (i.e.,
 297 500 samples). With longer lengths, the data distribution may converge to the Gum-

298 bel distribution [Gumbel, 1958; Coles, 2001], but the temporal resolution will de-
299 crease because relatively smaller peaks of CC values will be neglected if a higher
300 peak emerges in the same interval, which becomes likely for longer intervals. In con-
301 trast, with shorter lengths, the convergence might not be achieved, and the data
302 will require fitting using not the Gumbel (3) but the GEV (2) distribution, which
303 includes one more parameter and is time-consuming (Appendix C). Therefore, the
304 effect of the length should be quantified theoretically and practically in the future.

305 The background level of CC may have daily variation [Aso et al., 2011] or long-
306 term variation as shown in Figure 5, and, for precise analysis, the threshold should
307 be determined in each term (e.g., diurnal and nocturnal distribution of CC). In such
308 a case, our method can be applied to each term separately, although we ignored such
309 variations for simplicity.

310 Because we analyzed continuous records only from 4 stations, it remains un-
311 clear whether the empirical distribution can be modeled by the Gumbel distribution
312 in general cases. A suitable approximation is possible using other limits of GEV: the
313 Fréchet or Weibull distribution. In practice, the shape of the tail should be further
314 investigated considering these possibilities in each analysis.

315 5 Conclusion

316 We developed an objective matched-filter technique based on AIC and the ex-
317 treme value theory. We showed that the CC between any template and i.i.d. random
318 waveform follows the normal distribution, which provides a reference for examining
319 the deviation of data from the i.i.d. case. To reduce the possibility of a false posi-
320 tive, we considered the maximum of CC in each interval and found that the maxima
321 follows the Gumbel distribution. Finally, using the distribution and AIC, we propose
322 a reasonable method for detecting outlier seismic signals that is less sensitive to ar-
323 bitrariness than a conventional thresholding method. Regardless of whether NCC
324 follows the normal distribution, the proposed method can be applied to analyses of
325 seismic event detection.

326 **Acknowledgments**

327 We used continuous waveform records of the NIED high sensitivity seismograph net-
 328 work of Japan (<https://doi.org/10.17598/NIED.0003>) and JMA unified earthquake
 329 catalog(<https://www.hinet.bosai.go.jp/REGS/JMA/jmalist.php?LANG=en>). This
 330 work was supported by MEXT, under its Earthquake and Volcano Hazards Observa-
 331 tion and Research Program. Yutaka Toyomoto contributed to waveform picking and
 332 preliminary calculations. We thank Kazuaki Ohta, Naofumi Aso, Hiroyuki Noda and
 333 Toru Imai for helpful discussions.

334 **References**

- 335 Akaike, H. (1973). Information theory and an extension of the maximum likelihood
 336 principle, in *2nd International Symposium on Information Theory* pp.267–281,
 337 Akademiai Kiado.
- 338 Aso, N., Ohta, K., & Ide, S. (2011). Volcanic-like low-frequency earthquakes be-
 339 neath Osaka Bay in the absence of a volcano. *Geophys. Res. Lett.*, **38**(8), L08303.
 340 <http://doi.org/10.1029/2011GL046935>
- 341 Aso, N., Ohta, K., & Ide, S. (2013). Tectonic, volcanic, and semi-volcanic deep
 342 low-frequency earthquakes in western Japan. *Tectonophysics*, **600**, 27–40.
 343 <http://doi.org/10.1016/j.tecto.2012.12.015>.
- 344 Bouchon, M., Karabulut, H., Aktar, M., Özalaybey, S., Schmittbuhl, J., & Bouin,
 345 M. P. (2011). Extended nucleation of the 1999 Mw 7.6 Izmit earthquake. *Science*,
 346 **331**(6019), 877–880. <http://doi.org/10.1126/science.1197341>
- 347 Coles, S., (2001). *An introduction to statistical modeling of extreme values*, Springer-
 348 Verlag, London.
- 349 David, H. A., & Nagaraja, H. N. (2003). *Order statistics*, 3rd edn. Wiley Series in
 350 Probability and Statistics, John Wiley & Sons, New Jersey.
- 351 Doi, I., & Kawakata, H. (2012). A non-accelerating foreshock sequence followed by
 352 a short period of quiescence for a large inland earthquake. *Geophys. Res. Lett.*,
 353 **39**(11). <http://doi.org/10.1029/2012GL051779>
- 354 Doi, I., & Kawakata, H. (2013). Spatio-temporal occurrence patterns among the
 355 foreshocks preceding the 2007 Noto Hanto earthquake. *Earth Planets Space*, **65**(9),
 356 1053–1058. <http://doi.org/10.5047/eps.2013.04.001>

- 357 Gibbons, S. J., & Ringdal, F. (2006). The detection of low magnitude seismic
 358 events using array-based waveform correlation. *Geophys. J. Int.*, **165**(1), 149–166.
 359 <http://doi.org/10.1111/j.1365-246X.2006.02865.x>
- 360 Gumbel, E. J. (1958). *Statistics of Extremes*, Dover.
- 361 Hosking, J. R. M. (1990). L-moments: analysis and estimation of distributions us-
 362 ing linear combinations of order statistics, *J. Roy. Stat. Soc. B.* **52**(1) 105–124.
 363 <https://doi.org/10.1111/j.2517-6161.1990.tb01775.x>
- 364 Kadota, K., Nishimura, S.-I., Bono, H., Nakamura, S., Hayashizaki, Y., Okazaki, Y.,
 365 & Takahashi, K. (2003). Detection of genes with tissue-specific expression patterns
 366 using Akaike’s information criterion procedure. *Physiol. Genomics*, **12**(3), 251–
 367 259. <http://doi.org/10.1152/physiolgenomics.00153.2002>
- 368 Kato, A., Obara, K., Igarashi, T., Tsuruoka, H., Nakagawa, S., & Hirata, N. (2012).
 369 Propagation of slow slip leading up to the 2011 Mw 9.0 Tohoku-Oki earthquake,
 370 *Science*, **335**, 705–708. <http://doi.org/10.1126/science.1215141>
- 371 Kitagawa, G. (1979). On the use of AIC for the detection of outliers. *Technometrics*,
 372 **21**(2), 193–199. <http://doi.org/10.1080/00401706.1979.10489749>
- 373 Marmolejo-Ramos, F., Vlez, J.I., & Romo, X. (2015). Automatic detection
 374 of discordant outliers via the Ueda’s method, *J. Stat. Distrib. App.*, **2**:8.
 375 <https://doi.org/10.1186/s40488-015-0031-y>
- 376 Martins, E. S., & Stedinger, J. R. (2000). Generalized maximum-likelihood general-
 377 ized extreme-value quantile estimators for hydrologic data, *Water Resour. Res.*,
 378 **36**(3) 737–744. <https://doi.org/10.1029/1999WR900330>
- 379 Maxwell, J. C. (1860). V. Illustrations of the dynamical theory of gases. –Part I.
 380 On the motions and collisions of perfectly elastic spheres, The London, Edin-
 381 burgh, and Dublin Philosophical Magazine and Journal of Science, 19(124), 19–32.
 382 <https://doi.org/10.1080/14786446008642818>
- 383 Ohmi, S. (2015). Seismic activity near Mt. Hotaka in Hida mountain range in 2013,
 384 detected by the matched filter method. *Zisin, Series 2*, **68**(1), 1–15. (in Japanese
 385 with English abstract) <https://doi.org/10.4294/zisin.68.1>
- 386 Ohta, K., & Ide, S. (2008). A precise hypocenter determination method using net-
 387 work correlation coefficients and its application to deep low-frequency earth-
 388 quakes. *Earth Planets Space*, **60**(8), 877–882. <http://doi.org/10.1186/BF03352840>

- 389 Shelly, D. R., Beroza, G. C., & Ide, S. (2007). Non-volcanic tremor
 390 and low-frequency earthquake swarms. *Nature*, **446**(7133), 305–307.
 391 <http://doi.org/10.1038/nature05666>
- 392 Shimijo, K., Enescu, B., Yagi, Y., & Takeda, T. (2014). Fluid-driven seismicity ac-
 393 tivation in northern Nagano region after the 2011 M9.0 Tohoku-oki earthquake.
 394 *Geophys. Res. Lett.*, **41**(21), 7524–7531. <http://doi.org/10.1002/2014GL061763>
- 395 Squire, W., & Trapp, G. (1998). Using Complex Variables to Esti-
 396 mate Derivatives of Real Functions, *SIAM Rev.*, **40**(1) 110–112.
 397 <https://doi.org/10.1137/S003614459631241X>
- 398 Ueda, T. (1996). Simple method for the detection of outliers. *Japanese J. Appl.*
 399 *Stat.*, **25**(1), 17-26 (in Japanese). <https://doi.org/10.5023/jappstat.25.17>
- 400 Ueda, T. (2009). A simple method for the detection of outliers. *Electron. J. Appl.*
 401 *Stat. Anal.*, **1**, 67–76. (F. Marmolejo-Ramos & S. Kinoshita, Trans.) (Original
 402 work published in 1996) <http://doi.org/10.1285/i20705948v2n1p67>

403 **Appendix A Approximation of the CC distribution**

404 Here, we show that the normal distribution $\mathcal{N}(0, d^{-1})$ approximates the theo-
 405 retical distribution of CC between d -dimensional two vectors \mathbf{u} and \mathbf{v} extracted from
 406 a continuous waveform record. First, we show that the extracted vector is statisti-
 407 cally isotropic. From the definition, we consider $\mathbf{v}^{(t)} = (x_t, x_{t+1}, \dots, x_{t+d-1})$, where
 408 x_t is the t -th component of continuous record. Therefore, $CC_t = \hat{\mathbf{u}} \cdot \hat{\mathbf{v}}^{(t)}$ is the t -th
 409 value of CC if \mathbf{u} is the fixed template. If $t_0 \in [t, t + d - 1]$ exists such that $|x_{t_0}|$ is
 410 significantly larger (or smaller) than others, $\hat{\mathbf{v}}^{(t)}$ itself is strongly (or less) oriented
 411 to the t_0 -th direction. However, simultaneously, $\hat{\mathbf{v}}^{(t+1)}, \hat{\mathbf{v}}^{(t+2)}, \hat{\mathbf{v}}^{(t+3)} \dots$ are strongly
 412 (or less) oriented towards the $t_0 - 1, t_0 - 2, t_0 - 3 \dots$ direction; this discussion is ob-
 413 viously valid even if the continuous record has some self-interdependency. Therefore,
 414 it is impossible to give some tendency to the direction of \mathbf{v} , that is, $\mathbf{v}^{(t)}$ for all t is
 415 statistically isotropic.

416 Given the isotropy, the normal distribution $\mathcal{N}(0, d^{-1})$ can be obtained as the
 417 extension of the derivation of the Maxwell-Boltzmann distribution. However, Maxwell
 418 (1860) assumed that each component of the vector, which is 3-dimensional and d -
 419 dimensional in the original and our problem, respectively, is independent; in our
 420 problem, this assumption does not hold because of $|\hat{\mathbf{u}}|^2 = |\hat{\mathbf{v}}|^2 = 1$, where $\hat{\mathbf{u}}$ and

421 $\widehat{\mathbf{v}}$ are normalized \mathbf{u} and \mathbf{v} , respectively, after elimination of their offset. Therefore,
 422 we loosen this constraint as $E(|\widehat{\mathbf{v}}|^2) = 1$, where $E(\cdot)$ indicates the mean value.
 423 After the derivation, we justify this assumption for larger value of d .

424 The derivation of the Maxwell-Boltzmann distribution is purely mathematical
 425 rather than physical. Maxwell [1860] considered that each component of particle ve-
 426 locity $\mathbf{v} = (v_1, \dots, v_d)$ is a random variable that follows the same PDF, P . Although
 427 only $d = 3$ was considered in the original, we extend it into the general case. In the
 428 following, we consider the PDF for each component of $\widehat{\mathbf{v}} = (\widehat{v}_1, \dots, \widehat{v}_d)$.

By assuming that the random vector \mathbf{v} is statistically isotropic (i.e., “*the direc-
 tions of the coordinates are perfectly arbitrary*”, Maxwell wrote), $E(\widehat{v}_j) = 0$ holds
 for arbitrary direction, and the joint probability of $\widehat{v}_1, \dots, \widehat{v}_d$ is coordinate-free and
 depends only on $|\widehat{\mathbf{v}}|^2$ written as

$$\prod_{j=1}^d P(\widehat{v}_j) = \phi \left(\sum_{j=1}^d \widehat{v}_j^2 \right). \quad (\text{A.1})$$

Because only an exponential function satisfies this property,

$$P(\widehat{v}_j) = \frac{1}{\alpha\sqrt{\pi}} \exp \left(-\frac{\widehat{v}_j^2}{\alpha^2} \right) \quad (\text{A.2})$$

is obtained under the condition of $\int_{\mathbb{R}} P(x) dx = 1$, where α is a positive parameter to
 be determined. The joint probability is written as

$$\prod_{j=1}^d P(\widehat{v}_j) = \frac{1}{\alpha^d \pi^{d/2}} \exp \left(-\frac{|\widehat{\mathbf{v}}|^2}{\alpha^2} \right), \quad (\text{A.3})$$

and the mean value of $|\widehat{\mathbf{v}}|^2$ is

$$E(|\widehat{\mathbf{v}}|^2) = \int_{\mathbb{R}^d} |\widehat{\mathbf{v}}|^2 \prod_{j=1}^d P(\widehat{v}_j) d\widehat{v}_j \quad (\text{A.4})$$

$$= \frac{1}{\alpha^d \pi^{d/2}} \int_{S_{d-1}} d\omega \int_0^\infty |\widehat{\mathbf{v}}|^2 |\widehat{\mathbf{v}}|^{d-1} \exp \left(-\frac{|\widehat{\mathbf{v}}|^2}{\alpha^2} \right) d|\widehat{\mathbf{v}}| \quad (\text{A.5})$$

$$= \frac{2\pi^{d/2}}{\alpha^d \pi^{d/2} \Gamma(d/2)} \frac{1}{2} \alpha^{d+2} \Gamma \left(\frac{d}{2} + 1 \right) \quad (\text{A.6})$$

$$= \frac{\alpha^2 d}{2}, \quad (\text{A.7})$$

where $S_{d-1} = 2\pi^{d/2}/\Gamma(d/2)$ is the area of $(d-1)$ -dimensional unit sphere, $d\omega$ is the
 solid angle, and Γ is the Gamma function. $|\widehat{\mathbf{v}}|^{d-1}$ is derived from the Jacobian, and
 we use

$$\int_0^\infty x^p \exp \left(-\frac{x^2}{a^2} \right) dx = \frac{1}{2} a^{p+1} \Gamma \left(\frac{p+1}{2} \right). \quad (\text{A.8})$$

Finally, with $E(|\hat{\mathbf{v}}|^2) = 1$, we get

$$\alpha^2 = \frac{2}{d}, \quad (\text{A.9})$$

which yields

$$P(\hat{v}_j) = \sqrt{\frac{d}{2\pi}} \exp\left(-\frac{\hat{v}_j^2}{2d^{-1}}\right). \quad (\text{A.10})$$

Obviously, if d is small, eq.(A.10) does not approximate the distribution of CC because the probability is not negligible for $|\hat{v}_j| > 1$. Hence we have to consider the sufficiently large value of d that makes $P(|\hat{v}_j| > 1)$ negligibly small. Moreover, the variance of $|\hat{\mathbf{v}}|^2$ calculated as

$$E\left((|\hat{\mathbf{v}}|^2 - 1)^2\right) = E(|\hat{\mathbf{v}}|^4) - 2E(|\hat{\mathbf{v}}|^2) + E(1) \quad (\text{A.11})$$

$$= \alpha^4 \left(\frac{d}{2} + 1\right) \frac{d}{2} - 2 + 1 \quad (\text{A.12})$$

$$= \frac{2}{d}, \quad (\text{A.13})$$

429 means that the possibility of $|\hat{\mathbf{v}}|^2 = 1$ in the strict sense becomes larger as d in-
 430 creases. Therefore, the constraint $|\hat{\mathbf{v}}|^2 = 1$ is approximately satisfied for larger values
 431 of d .

432 Considering that both Maxwell's particle and our unit random vector is isotropic,
 433 the PDF (A.10) provides not only the specific component \hat{v}_j but also a component
 434 along all directions including $\hat{\mathbf{u}}$ in the same manner. Therefore, the inner product of
 435 an arbitrary random unit vector $\hat{\mathbf{v}}$ extracted from random continuous waveform and
 436 arbitrary fixed unit vector $\hat{\mathbf{u}}$ approximately follows the normal distribution with the
 437 variance of d^{-1} .

438 **Appendix B Does not the log-likelihood vary significantly after** 439 **elimination of some data?**

440 In eq.(5), we assume that the maximum likelihood parameters for all N , $N - s$
 441 and $N - s - 1$ data do not vary significantly because $N \gg s$ holds. Even so, the
 442 effect of the small difference of the parameters on AIC_s appears to be unclear. In
 443 the calculation of the log-likelihood, $\sum_{j=s+1}^N \log P(x_j | \mu', \sigma')$, even negligibly small
 444 difference could be stacked and possibly become a significant amount.

However, we can show that the stacked amount is still negligible. Let the pa-
 rameters (μ', σ') and (μ'', σ'') be the MLE using all N data and $N - s$ data, respec-

tively. Therefore, the error of AIC (i.e., error of the log-likelihood) using the former instead of latter has the same order of the Kullback–Leibler divergence

$$D(P_G(\mu'', \sigma''), P_G(\mu', \sigma')) = \int_{\mathbb{R}} P_G(x | \mu'', \sigma'') \log \frac{P_G(x | \mu'', \sigma'')}{P_G(x | \mu', \sigma')} dx. \quad (\text{B.1})$$

445 This is equivalent to the loss function defined in eq.(3.1) of Akaike [1973], and de-
 446 pends only on the second or higher order of $(\mu'' - \mu')$ and $(\sigma'' - \sigma')$ after the Taylor
 447 series expansion; see eq.(4.5) of Akaike [1973]. Hence, any small error of $(\mu'' - \mu')$ or
 448 $(\sigma'' - \sigma')$ does not vary the log-likelihood significantly.

449 Appendix C MLE of GEV parameters

MLE of GEV parameters is equivalent to solving the equations below with respect to $\mu', \sigma',$ and k :

$$\begin{aligned} \sum_{i=1}^N \frac{z_i}{y_i} &= 0, \\ -N + \sum_{i=1}^N \frac{z_i}{y_i} \left(\frac{x_i - \mu'}{\sigma'} \right) &= 0, \\ \sum_{i=1}^N \left(z_i \log(y_i) + \frac{z_i}{y_i} \left(\frac{x_i - \mu'}{\sigma'} \right) \right) &= 0 \end{aligned} \quad (\text{C.1})$$

450 [Martins & Stedinger, 2000; Coles, 2001], where $y_i := 1 + (k/\sigma')(x_i - \mu')$ and
 451 $z_i := 1 + k - y_i^{-1/k}$ (note: k is opposite in sign between Coles [2001] and Mar-
 452 tins & Stedinger [2000]), and we eliminate some unnecessary coefficients. To solve
 453 them using the Newton-Raphson method, the Hessian matrix that is the deriva-
 454 tive of eqs.(C.1) with respect to the 3 parameters should be calculated. Although
 455 the representations of the derivatives are slightly complicated, we simply compute
 456 the matrix by the automatic differentiation using a small complex variable [Squire
 457 & Trapp, 1998]. The initial values for iteration are given by L -moments [Hosking,
 458 1990].

459 Unfortunately, the Newton-Raphson method sometimes fails during its itera-
 460 tion due to the following reason. During the MLE process, we have to calculate the
 461 log-likelihood $\log P_{\text{GEV}}(x_j | \mu', \sigma', k)$ for all the sample x_j , where μ', σ', k is not nec-
 462 essarily the MLE of the parameters, which is attributable to the iteration. In case
 463 of $k < 0$, as mentioned in the main text, the PDF, P_{GEV} , for $x > \mu - \sigma'/k$ is zero.
 464 Therefore, we may substitute zero into P_{GEV} if $x_j > \mu - \sigma'/k$ holds, and the itera-
 465 tion stops due to the numerical error ($\log 0 = -\infty$). In particular, this error tends to

466 occur if the sample includes outliers, which is abnormally large. Hence, the MLE of
 467 GEV parameters is technically difficult, and we may require some ad hoc implemen-
 468 tation.

Because we particularly focus on the case of the Gumbel distribution, the equations for maximum likelihood estimators are represented explicitly by taking $k \rightarrow \infty$:

$$\begin{aligned} \sum_{i=1}^N \left(1 - \exp \left(-\frac{x_i - \mu'}{\sigma'} \right) \right) &= 0, \\ -N + \sum_{i=1}^N \left(1 - \exp \left(-\frac{x_i - \mu'}{\sigma'} \right) \right) \left(\frac{x_i - \mu'}{\sigma'} \right) &= 0. \end{aligned} \tag{C.2}$$